FINAL REPORT

FEASIBILITY ANALYSIS OF RECIPROCATING MAGNETIC HEAT PUMPS

By
A. V. Larson
J. G. Hartley
Sam V. Shelton
M. M. Smith

Prepared for
NATIONAL AERONAUTICS AND SPACE ADMINISTRATION
LEWIS RESEARCH CENTER
CLEVELAND, OHIO 44135

Under
NASA Grant NAG-3-600

December 1989

GEORGIA INSTITUTE OF TECHNOLOGY
A Unit of the University System of Georgia
THE GEORGE W. WOODRUFF SCHOOL OF MECHANICAL ENGINEERING
ATLANTA, GEORGIA 30332-0405

FEASIBILITY ANALYSIS OF RECIPROCATING MAGNETIC HEAT PUMPS

By
A. V. Larson, Co-P.I.
J. G. Hartley, Co-P.I.
Sam V. Shelton, Co-P.I.
M. M. Smith

FINAL REPORT
for the period July 1985 to July 1986

Prepared for
NATIONAL AERONAUTICS AND SPACE ADMINISTRATION
LEWIS RESEARCH CENTER
CLEVELAND, OHIO 44135

Under
NASA Grant NAG-3-600

December 1989

GEORGIA INSTITUTE OF TECHNOLOGY
A Unit of the University System of Georgia
THE GEORGE W. WOODRUFF SCHOOL OF MECHANICAL ENGINEERING
ATLANTA, GEORGIA 30332-0405

ABSTRACT

A reciprocating Gadolinium core in a regeneration fluid column in the warm bore of a superconducting solenoidal magnet is considered for magnetic refrigeration in 3.517 MW (1000 ton) applications. A procedure is presented to minimize the amount of superconducting cable needed in the magnet design. Estimated system capital costs for an ideal magnetic refrigerator of this type become comparable to conventional chillers as the frequency of reciprocation approaches 10 Hertz. A one-dimensional finite difference analysis of a regenerator cycling at 0.027 Hertz is presented which exhibits some of the features seen in the experiments of G.V. Brown.

The NASA Technical Officer for this grant is Gerald V. Brown, NASA LEWIS RESEARCH CENTER.

ACKNOWLEDGEMENTS

The authors wish to thank our colleague, J.W. Brazell, for discussions on the mechanical system; Betty Holtsinger for typing and proofing the manuscript; and students, Steven Corson and Michael L. Robertson for the drawings.

TABLE OF CONTENTS

NOMENCLATURE

A	Column cross-section; Ampere
B	Magnetic induction
B_o	Magnetic induction at magnet center
B_w	Magnet induction in central plane at wall of core
C	Cost of magnet and magnetic metal core
C_a	Cost of auxiliary equipment
C_m	Specific cost of magnetic metal
C_p	Specific heat at constant pressure
C_s	Specific cost of superconducting cable
C_{st}	Cost of magnet structural support
C_t	Total cost of system
C_1	Cost coefficient defined by eq. (16)
cv	Control Volume
F	Form factor defined by eq. (21)
f	Frequency of demagnetization (cycle frequency)
H	Magnetic intensity
Hz	Hertz (cycles/sec)
H^*	Enthalpy

h	Specific enthalpy
J	Globally averaged current density in magnet winding
J_{sa}	Characteristic current density of superconducting alloy
K	Unit of temperature, Kelvin
k	Thermal conductivity
L	Length of magnet winding
M	Magnetization
M_m	Mass of core magnetic metal
M_s	Mass of superconducting cable
N	Unit of force, Newton
R_i	Inner radius of magnet winding
R_o	Outer radius of magnet winding
P	Cost term defined by Eq. (19)
P_{min}	P at α_{min}
Q_L	Heat transfer to column end from source
Q_H	Heat transfer from column end to sink
$\dot{Q}_L$	Refrigeration load rate
$\dot{Q}_{in}$	Thermal input power
$\dot{Q}_{out}$	Thermal output power

q_L	Specific refrigeration capacity of magnetic metal
s	Specific entropy
T	Temperature; Unit of magnetic field, Tesla
t	Time
U	Internal energy
V	Speed of core relative to column
V_b	Volume of magnet bore
V_{abs}	Speed of core relative to magnet
V_{col}	Speed of column relative to magnet
V_f	Speed of fluid in core, relative to column
V_s	Volume of superconducting cable
V_{sa}	Volume of superconducting alloy in cable
V_w	Volume of magnet windings including spacing
v	Specific volume
W	Unit of power, Watt
X	Coordinate relative to magnet
x	Coordinate relative to column

Greek Symbols

α	Ratio of outer to inner radii for magnet winding
β	Ratio of length to inner diameter for magnet winding
β_{min}	Value of β at α_{min}
δ	Fraction of winding volume filled by superconducting alloy
δ_s	Fraction of winding volume filled by superconducting cable
δ_{sa}	Fraction of cable cross-section filled by superconducting alloy
ϵ	Porosity defined by A_f/A
γ	Fraction of core filled by magnetic metal
ρ	Density
ρ_m	Density of magnetic metal (non-porous form)
ρ_s	Density of superconducting cable
μ_o	Magnetic permeability of vacuum

Subscripts

H	high
L	low
f	fluid
m	magnetic metal
min	minimum

I. INTRODUCTION

Some materials become hotter (cooler) when magnetized (demagnetized). Refrigerators and heat pumps based on the effect can be imagined in principle. In practice, adiabatic demagnetization has been important in cooling below a few degrees Kelvin. This report considers the feasibility of commercial application of a magnetocaloric refrigerator operating near room temperature. The motivation is to find devices of greater capacity, economy or design flexibility than are found in conventional technology to meet particular applications.

In 1976, Brown [1,2] at NASA/Lewis suggested the possibility of practical magnetocaloric devices at normal temperatures. The bulk availability of rare-earths such as gadolinium and the advent of higher field superconducting magnets with considerably less power consumption was intriguing because the magnetocaloric effect is stronger near the Curie point (Gd 293K) and with larger field changes.

Brown discussed several possible thermodynamic cycles and selected the magnetic Stirling cycle with regeneration for further study. A proof of concept laboratory device was successfully demonstrated [3]. The commercial feasibility was thought to rest on economics and the thermodynamic performance of the regenerator. These are the factors addressed in this paper.

Comparisons are made here on the capital and operating costs of conventional 1000 ton chillers and a system using a reciprocating porous gadolinium core in a fluid regenerating column.

Progress is reported on modelling the gadolinium - fluid column regenerator. This modelling is to eventually take into account rate dependent and irreversible processes, but hasn't done so yet.

II. BACKGROUND

Magnetic Cooling Devices

The magnetocaloric effect was first observed by Weiss and Piccard [4] in 1918. Prior to this Edison [5] and Tesla [6] had patented designs for refrigerators and engines based on the ferromagnetic-paramagnetic transition.

Temperatures down to 1 K can be obtained to liquefy He. Debye [7] in 1926 and Giauque [8] in 1927 independently suggested that lower temperatures could be produced by the adiabatic demagnetization of a paramagnetic substance. The method was successfully tested in 1933 by Giauque and MacDougall [9]. Adiabatic demagnetization has been used since then in low-temperature research.

In "one-shot" devices a paramagnetic substance is placed in thermal contact with a low temperature reservoir of He and a material to be studied at low temperature. An applied magnetic field causes thermal energy to flow from the paramagnetic material into the reservoir. Once thermal equilibrium is established the thermal contact to the reservoir is broken and the magnetic field is lowered to zero. The experimental material and the paramagnetic substance will then drop to a temperature below that of the reservoir.

Refrigerators have been built using paramagnetic substances to maintain temperatures below 1 K for loads less than 1 mW [10, 11]. There is substantial interest in using similar devices to maintain low temperatures (1 to 20 K) in superconducting devices and to cool instruments in space craft [13, 14, 15]. These devices would need to handle loads greater than 1 W.

There are basically two competing designs in current magnetic refrigeration research at temperatures above 1 K. One involves a porous magnetic material moving with a reciprocating motion in a fluid column. The other design uses a rotating wheel of magnetic material with a counterflowing fluid acting as the link between the source and sink. The two designs are referred to as the reciprocating and rotating designs, respectively. Both rotating and reciprocating magnetic heat pumps have been proposed for applications in space, laser amplifier cooling, helium liquefication and industrial waste heat recovery [13, 14, 15, 16, 17].

Reciprocating Magnetic Heat Pumps

The reciprocating magnetic heat pump consists in part of the porous magnetic material, a fluid-filled regenerator column and the external magnet. A typical cycle is shown in Fig. 1. Here, the magnet is on continuously.

In the mechanical cycle, process 1-2 includes magnetization of the magnetic material in the core. In the isofield process 2-3 the material is cooled. The cycle is completed by core demagnetization 3-4 and an isofield increase in temperature 4-1. In practice, the necessary translation would likely be vertical for proper fluid control. At steady operating conditions the fluid in the regenerator column is stratified with respect to temperature and has an overall temperature difference of $T_H - T_L$. In the column shown in Fig. 1 the left end is hot. The motion of the magnetic material with respect to the magnet is not always required. Instead, the magnet could be turned on and off with the magnetic material inside the bore. However, the nature of high-field superconducting magnets may favor the use of relative motion and a constant field.

The details of the actual energy addition and rejection processes at the ends of the regenerator column are not shown. Various methods could be used, and these, along with the details of the relative motion and the spatial variation in the magnetic field, will determine what type thermodynamic cycle is achieved. Fig. 2 shows a cycle consisting of two isothermal and two

isofield paths which is the representation of the cycle considered here. If regeneration paths 2-3 and 4-1 were congruent as suggested by the dashed line, then the ideal cycle would have the same coefficient of performance as the Carnot device. (The dashed path could be achieved in practice by programming the partial magnetization of the core during warming, which is not considered initially.)

The reciprocating magnetic heat pump was first proposed by J. R. Van Geuns in 1966 [18]. More recently this device has been discussed in several papers by G. V. Brown [1, 2, 19]. Brown and Papell [3] have built and tested a small reciprocating magnetic device with adiabatic walls (no source or sink). The maximum field employed was 7 T producing a maximum temperature span of about 80 K. In separate tests the lowest and highest temperatures attained were 241 K and 328 K. Two factors which would limit the performance of an actual refrigerator were noted. The successful operation of a reciprocating refrigerator depends on the maintenance of a temperature gradient in the fluid, but the gradient in the test device was degraded by jets of fluid issuing from the core causing fluid mixing in the region behind it. Also, more surface area was needed to enhance heat transfer.

Two other reciprocating magnetic refrigerators have been tested. Barclay et al. [20] built and tested a device which operated at source and sink temperatures of 2.2 K and 4.2 K, respectively. These limiting factors were noted: (1) frictional heating (mechanical contact), (2) viscous heating, and

(3) mixing owing to the motion of the porous core. C. Delpuech et al. [21] tested a double acting reciprocating magnetic refrigerator in 1981. This device has two paramagnetic cores and magnets. The cold section is located at the middle of the regenerator column and thermal energy is rejected from each end. The refrigerator was tested between 1.8 K and 4.2 K and produced nearly one-half watt of refrigeration capacity.

Rotating Magnetic Heat Pumps

The rotating magnetic refrigerator is arranged as a counterflow heat exchanger as illustrated in Fig. 3. The rim of the wheel is composed of porous magnetic material. Fluid is pumped through the porous rim as it rotates through high-field and low-field regions.

A prototype to test the rotary magnetic heat pump principle was designed, built and tested in 1977 [22]. This device operated at room temperature and was a forerunner of a room temperature device that was reported on in 1981 [23]. Also, a rotating magnetic refrigerator operating between about 2 K and 4 K has been tested [24].

The two main problems with rotary designs are obtaining a high concentrated field at one location on the wheel and a zero field elsewhere, and controlling the flow of the fluid. These problems, along with lower than expected heat transfer between the fluid and magnetic material, resulted in a refrigeration capacity of 400 W, a Coefficient of Performance (COP) of 26

percent of the Carnot COP and a maximum ΔT of 7 K as compared to design goals of 1000 W, 70 percent and 40 K, respectively [23]. Barclay [25] has suggested that the flow problem might be alleviated somewhat by using a ferrofluid which would be driven through the porous material by magnetic forces.

A Different Magnetic Heat Pump

One other current device using magnetic materials, that does not fall into the previous two categories, is described in a 1984 patent by H. Nakagome and T. Hashimoto [26]. They envision a refrigerator composed of a magnetic material connected to one-way heat pipes. No published accounts of an operating device have been located.

III. ECONOMIC ESTIMATES

Capital Cost Model

To obtain economic estimates the basic system of Fig. 1 with a steady magnet and a reciprocating magnetic porous core was chosen. Some simplifying assumptions were made.

1) The porous core just fills the bore of the magnet windings.
2) The vacuum field of the magnet is uniform in the bore with a value equal to that calculated for the magnet center.

3) Any metallic piece of magnetic core responds to the uniform applied field in the same manner as the center element of a long thin ellipsoid. Demagnetization is negligible.

4) The magnet is assembled by stacking thin disk-shaped coils with adequate voids for cooling channels and structural members.

5) The vacuum field at the magnet center is calculated using a global spatially averaged uniform current density.

6) The refrigeration rate is proportional to the frequency of demagnetization of the core.

7) Eddy currents are ignored.

8) The coefficient of performance is the maximum COP: There are no irreversibilities.

The logic that follows starts with a load specification. Then the amount of magnetic material to satisfy the load requirement is found. Finally after the superconducting cable is chosen, the shape of the magnet solenoid is optimized to provide the necessary field at minimum cable weight (for a uniform winding).

The refrigeration rate is

$$\dot{Q}_L = q_L M_m f \tag{1}$$

where q_L is the refrigeration capacity per unit mass of core magnetic metal per each demagnetization,

M_m is the mass of the core magnetic metal, and

f is the frequency of demagnetization.

Therefore the required volume of the magnetic material is

$$V_m = \frac{\dot{Q}_L}{q_L \; f \; \rho_m} \tag{2}$$

where ρ_m is the density of the magnetic metal in non-porous form. Allowing for the porosity of the core,

$$V_m = \gamma \; V_b \tag{3}$$

where V_b is the volume of the magnet bore, and

γ is the filling fraction of the magnetic metal in the core.

The magnet is illustrated in more detail in Fig. 4

where R_o is the outer radius of the winding,

R_i is the inner radius of the winding,

L is the length of the winding,

J is the globally averaged current density, and

$B_o = B_w = B$ is assumed.

Defining

$$\alpha \equiv \frac{R_o}{R_i} \tag{4}$$

$$\beta \equiv \frac{L}{2R_i} \tag{5}$$

it follows that

$$V_b = 2\pi \; R_i^3 \; \beta. \tag{6}$$

The windings and their spacing occupy a volume, V_w given by

$$V_w = (\alpha^2 - 1)\, V_b. \tag{7}$$

The superconducting cable has a volume V_s

$$V_s = \delta_s\, V_w \tag{8}$$

where δ_s is the fraction of the winding volume filled with superconducting cable.

A typical superconductor cable consists of tiny filaments of superconducting alloy embedded in copper. For the purposes here, it is necessary to specify the cable in more detail. Let δ_{sa} be the fraction of the cable cross-section which is superconducting alloy, then

$$V_{sa} = \delta_{sa}\, V_s \tag{9}$$

where V_{sa} is the volume of the superconducting alloy.

Defining $$\delta \equiv \delta_{sa}\, \delta_s \tag{10}$$

then $$V_{sa} = \delta V_w. \tag{11}$$

Now the global average current density J can be related to the known superconducting alloy characteristic current density, J_{sa}.

$$J = \delta\, J_{sa} \tag{12}$$

A complication arises in that q_L and J_{sa} each depend on the field.

$$J_{sa} = J_{sa}(B) \tag{13}$$

$$q_L = q_L(B,\, T_L) \tag{14}$$

Thus one must choose B, then find the volume of magnetic material, V_m, through equation (2), then proceed to find the optimum winding shape starting with equations (13) and (12).

Since V_m and V_{sa} (expected to be high cost variables) are coupled by B one may seek to estimate the system cost as a function of B.

Let C_t be the total cost of the system

$$C_t = C_m M_m + C_s M_s + C_{st} + C_a \tag{15}$$

where C_m is the specific cost of the magnetic metal,

C_s is the specific cost of the superconducting cable,

C_{st} is the cost of the magnet structure, and

C_a is the cost of the auxiliary equipment.

Assume

$$C_{st} + C_s M_s = C_1 C_s M_s. \tag{16}$$

Define

$$C \equiv C_m \rho_m V_m + C_1 C_s \rho_s V_s \tag{17}$$

where ρ_m is the density of the magnetic material in non-porous form, and

ρ_s is the density of the superconducting cable.

Rewrite equation (17) using equations (3), (7) and (8):

$$C = C_m \rho_m V_m [1 + P] \tag{18}$$

where

$$P = \left[\frac{C_1 C_s \rho_s \delta_s}{C_m \rho_m \gamma}\right] (\alpha^2 - 1). \tag{19}$$

Cost Minimization Logic

Recall equation (2).

$$V_m = \frac{\dot{Q}_L}{f\, q_L \rho_m}$$

The application fixes $\dot{Q}_L$, T_L.

Choose the frequency, f, and the magnetic metal, ρ_m.

Choose B which fixes $q_L = q_L\,(B, T_L)$.

Now V_m is fixed in equations (2) and (18).

Choose the cable: C_s, ρ_s, δ_{sa}.

Choose the filling fractions: γ, δ_s.

B also fixes $J_{sa} = J_{sa}(B)$.

Now one can minimize the cost C of the magnet and magnetic material for given field B by minimizing $C_1\,(\alpha^2 - 1)$ in equations (19) and (18).

Assuming that C_1 is not a sensitive function of the design variables, one seeks to minimize α for a given B.

Minimum Radius Ratio, α

Following Reference [28] for this type magnet we have

$$B = J\, R_i\, F \tag{20}$$

where F is a form factor

$$F = F(\alpha,\beta)$$

$$F \equiv \mu_o \beta \ln \left\{ \frac{\alpha + (\alpha^2 + \beta^2)^{1/2}}{1 + (1 + \beta^2)^{1/2}} \right\} \tag{21}$$

where μ_o is the magnetic permeability of vacuum.

In equations (20) and (21), B and J have been fixed. The parameters α, β relate only to the shape of the magnet: R_o, R_i, L. One seeks to find the shape which minimizes α subject to the constraints of equations (20) and (21). The latter can be recast in an informative manner. Combine equations (3), (6), (12), (20) and (21) to get:

$$\frac{\beta}{F^3} = \left(\frac{\delta^3}{2\pi\gamma}\right)\left(V_m\right)\left(\frac{J_{sa}}{B}\right)^3 \tag{22}$$

or, using equation (2)

$$\frac{\beta}{F^3} = \left(\frac{\delta^3}{2\pi\gamma}\right)\left(\frac{\dot{Q}_L}{f}\right)\left(\frac{1}{q_L \rho_m}\right)\left(\frac{J_{sa}}{B}\right)^3 . \tag{23}$$

Since the parameters on the right have been fixed,

$$\frac{\beta}{F^3} = \text{constant.} \tag{24}$$

From equation (21), β/F^3 is a function only of α and β.

One can easily find α_{min} subject to the constraint in equation (24). A typical curve for α vs β is shown in Fig. 5. Now let β_{min} stand for the value of β associated with α_{min}.

Optimum Magnet Dimensions

Combine equations (3) and (6) after inserting the values for α_{min}, β_{min} to get

$$R_i = \left(\frac{V_m}{2\pi \gamma \beta_{min}} \right)^{1/3} . \tag{25}$$

From equation (4)

$$R_o = \alpha_{min} R_i . \tag{26}$$

The "build" of the winding defined as $R_o - R_i$, is

$$R_o - R_i = R_i (\alpha_{min} - 1). \tag{27}$$

From equation (5),

$$L = 2 \beta_{min} R_i . \tag{28}$$

Of course the inner and outer diameters are

$$D_i = 2 R_i \tag{29}$$

$$D_o = 2 R_o . \tag{30}$$

Input Data Case I

For the parameters of equation (23),

Load Requirements:

$\dot{Q}_L$ = 3517 kw (1000 Tons of Refrigeration)

f = 1Hz

Geometric Design:

γ = .8

δ = .1125 (δ_s = .9, δ_{sa} = .125)

Magnetic Metal: Gadolinium

$\rho_m = 7.9 \times 10^3$ Kg/m^3

C_m = \$200/Kg

$q_L = [.589B - .0817\ B^{3/2}]$ KJ/Kg at T_L = 280K

B in Tesla, Ref. [29].

Superconducting Cable:

1 part superconducting alloy, 7 parts copper

$\rho_s = 8.6 \times 10^3$ Kg/m^3

C_s = \$66/Kg, Ref. [30].

Superconducting Alloy:

$J_{sa} = J_{sa}(B)$ as given below.

$J_{sa} = (5.90)10^{10}\ (.773)^B$ Amp/m^2,

for B in the range 2.5T $\leq$ B $\leq$ 12T. Ref [31].

Cost Formula - Equations (18) and (19):

$C_m\rho_m = 1.58 \times 10^6$ \$/m^3

$C_s\rho_s = .568 \times 10^6$ \$/m^3.

Equation (18) becomes

$$C = \$(1.58E6)\ [1 + P_{min}]\ V_M, \tag{31}$$

Where P_{min} is given by setting $\alpha = \alpha_{min}$ in equation (19).

Equation (19) becomes

$$P = (.404)C_1\ (\alpha_{min}^2 - 1). \tag{32}$$

In the above, the cost of the Gd is:

$$\$(1.58E6)V_M \tag{33}$$

The cost of the superconducting cable is:

$$\$(1.58E6)V_M \frac{P}{C_1}. \tag{34}$$

The cost of the superconducting magnet is:

$$\$(1.58E6)V_M\ P. \tag{35}$$

Input Data Case II

The only change made for the second evaluation was to increase the frequency by a factor of 10.

Results

The results of the calculations for the costs of the Gadolinium and the cable are given in Tables 1 and 2, along with estimates for the costs of the magnet and the auxiliary equipment [30].

The magnet cost estimates have a large uncertainty because of the lack of appropriate data. There are commercial warm bore magnets for the Magnetic Resonance Imaging and other applications of about the same bore diameter and length as those in Tables 1 and 2. The MRI costs are strongly escalated by the need for field homogeneity over a relatively large volume. Field homogeneity is probably not so critical in magnetic heat pumps. On the other hand, the cost of the latter will escalate due to the need of the magnet to withstand large internal forces as the Gadolinium is withdrawn from the magnet.

For the cost of the magnet, $C_s + C_{st}$, we have simply used the expression:

$$C_s + C_{st} = \$(14B + 19)k \quad , \quad B \text{ in Tesla.}$$

This cost formula fits fairly well to marketed non-MRI magnets with bore shape and size similar to those of Tables 1 and 2. The \$19k represents the costs of a rack of electronics and a closed-loop liquid helium refrigeration system, both used for the operation of the magnet. The costs reflect small quantity production and do not include the significant reductions expected from high quantity manufacturing.

Table 1. Capital Cost Estimates Vs. Applied Field, f = 1 Hz.

	3T	6T	9T	12T
V_m, m^3	.3315	.1908	.1438	.1212
β/F^3, A^6/N^3	7.036E25	4.970E23	1.093E22	3.819E20
α_{min}	1.00265	1.01384	1.04972	1.15458
β_{min}	1.4	1.4	1.45	1.5
R_i, cm	36.12	30.04	27.02	25.24
R_o-R_i, cm	.0957	.416	1.112	3.90
L, cm	101.1	84.1	78.4	75.7
Cost, Gd $	524k	301k	227k	192k
Cost, Cable, $	1.1k	3.4k	9.4k	25.8k
Cost of Magnet, s	61k	103k	145k	187k
Cost of Auxiliaries	30k	30k	30k	30k
Cost of System, $	615k	434k	402k	409k

Table 2. Capital Cost Estimates vs. Applied Field, f = 10 Hz

	3T	6T	9T	12T
V_m, m^3	.03315	.01908	.01438	.01212
β/F^3, A^6/N^3	7.036E24	4.970E22	1.093E21	3.819E19
α_{min}	1.00572	1.02991	1.10808	1.3425
β_{min}	1.4	1.45	1.5	1.65
R_i, cm	16.76	13.77	12.39	11.34
R_o-R_i, cm	.0959	.419	1.339	3.89
L, cm	46.9	39.9	37.2	37.4
Cost, Gd, $	52.4k	30.1k	22.7k	19.2k
Cost, Cable, $	.2k	.7k	2.1k	6.2k
Cost of Magnet, $	61k	103k	145k	187k
Cost of Auxiliaries, $	30k	30k	30k	30k
Cost of System, $	143k	163k	198k	236k

Separately listed as auxiliary equipment is the mechanical system required to drive the motion of the regenerator and the magnetic core. If the ideal magnetic refrigerator operates between 280K and 310K, the ideal COP is 9.33, and the work required for a 35.17 MW load at f = 1 Hz would be 377 kJ of work per cycle. If the stroke length were 1 m, then the average force would be on the order of 377 kN with a peak force about twice as high. At f = 10 Hz, the average level would be about 37.7 kN. Since the actual motion would be vertical, the weight of the Gadolinium must be added, which increases the estimated level about 8%.

Even the case with the greatest forces (B = 3T, f = 1) can be met with hydraulic piston/cylinders and electromagnetic actuators. A non-magnetic stainless steel rod of say 5 cm diameter would suffice as the major driver (one rod on each end of the metal core). If the rods had to traverse the fluid column, each would use only a small percentage of the volume available (an effect neglected in Tables 1 and 2). However, by using some kind of internal latching between the core and the regenerator walls in paths 1-2 and 3-4 (Fig. 1), it may be possible to have the major drivers attached to the ends of the regenerator column.

Another set of piston/cylinders, valves and rods (the minor drivers) are needed to move the column relative to the core in paths 2-3 and 4-1. The mechanical power requirements here are much smaller than for the major drivers. The initial costs estimated for the mechanical system are [39]:

	$ 6k	two cylinders
	4k	two pumps
	6k	valves
	4k	controller
	10k	miscellaneous
TOTAL	$ 30k	

Operating Cost

An ideal thermodynamic cycle has been assumed. The quantitative effects of irreversibilities due to core/fluid interactions, eddy currents in the Gadolinium and other causes have not been assessed yet. The irreversibilites do increase with cycle frequency and will offset to some extent the capital cost advantage of higher frequency observed in Tables 1 and 2.

A serious loss occurs in the mechanical system in the conversion of motor shaft power to cylinder rod power. In conventional systems this conversion efficiency is about 80% [39]. However, the existing trend in hydraulics to much better efficiencies by using higher pressures and very efficient pumps, motors, and valves looks very encouraging [39].

IV. REGENERATOR COLUMN

The conceptual design selected for detailed system analysis is the reciprocating core in a regenerative fluid column within the bore of a steady superconducting magnet as in Fig. 1. The analysis is the subject, in part, of a dissertation in progress by one of the authors [32]. The first task was to treat the regenerator fluid and core using a simplified one-dimensional, transient model.

The assumptions in the model are:

1. The core is assumed to have a porous structure composed of gadolinium having a uniform porosity.
2. Temperature gradients in the fluid and core normal to the direction of motion are negligible. The fluid and gadolinium in the core are in thermal equilibrium in any cross-section.
3. Viscous forces and inertial forces are ignored.
4. Fluid properties are independent of temperature.
5. The magnetic field intensity, H, is a known function of position and steady in time, and is taken to be the vacuum field of the magnet.
6. The entropy of the gadolinium is a known function of temperature and magnetic field intensity.
7. The gadolinium is rigid and the fluid is incompressible.

8. The velocity of the core with respect to the regenerator column is constant during core traversals in the column.

9. There is no dwell time. Either the core or column (or both) is in motion relative to the magnet at all times.

10. Any effects of magnetically induced eddy currents are negligible.

The thermodynamic properties of gadolinium are given by Griffel [33], Brown [2], and Benford and Brown [34]. The general thermodynamic relations for magnetic materials are given by Hatsopoulos and Keenan [35] and Booker [36]. The relation between the applied fields (no magnetic material present) and the internal fields in the gadolinium in place is taken to be that of an ellipsoid of gadolinium [37,38] with no demagnetization effect.

To write the energy balance, fix a reference frame (x) to the left end of the column in Fig. 1 and assume the Gd core is moving to the right with speed V. For a differential control volume located at x in this frame

$$\left.\frac{\partial U}{\partial t}\right|_{cv} = \dot{Q} + \dot{W} + \text{Net Enthalpy Input Rate} \tag{36}$$

$$\left.\frac{\partial U}{\partial t}\right|_{cv} \simeq \left.\frac{\partial H^*}{\partial t}\right|_{cv} = \rho_m A_m \Delta x \frac{\partial h_m}{\partial t} + \rho_f A_f \Delta x \frac{\partial h_f}{\partial t} \tag{37}$$

$$\dot{Q} = k_m A_m \left(\left.\frac{\partial T_m}{\partial x}\right|_{x + \Delta x} - \left.\frac{\partial T_m}{\partial x}\right|_{x} \right) + k_f A_f \left(\left.\frac{\partial T_f}{\partial x}\right|_{x + \Delta x} - \left.\frac{\partial T_f}{\partial x}\right|_{x} \right) \tag{38}$$

$$\dot{W} = A_m \mu_o \Delta x H \frac{dM}{dt} \tag{39}$$

$$\text{Net Enthalpy Input Rate} = -\left[h_{x+\Delta x} - h_x\right]_m \rho_m A_m V - \left[h_{x+\Delta x} - h_x\right]_f \rho_f A_f V_f \quad (40)$$

where U is the internal energy,

t is the time,

$\dot{Q}$ is the thermal power,

$\dot{W}$ is the rate of magnetic work,

H^* is the enthalpy,

h is the specific enthalpy,

m, f are subscripts for magnetic metal, fluid,

ρ is the density,

$A_{m,f}$ is the cross-section area of metal or fluid,

k is the thermal conductivity,

T is the temperature,

μ_0 is the magnetic permeability of free space,

H is the magnetic intensity,

M is the magnetization,

V is the metal speed, relative to the column, and

V_f is the fluid speed in the core, relative to the column.

In this model the two magnetic vectors are colinear.

Combining the equations, dividing by $A\Delta x$, and taking the limit, one obtains

$$\rho_m(1-\epsilon)\left[\frac{dh_m}{dt} - \mu_o v_m H \frac{dM}{dt}\right] + \rho_f C_{pf}\left[\epsilon \frac{\partial T_f}{\partial t} - (1-\epsilon)V \frac{\partial T_f}{\partial x}\right] =$$

$$k_m (1-\epsilon) \frac{\partial^2 T_m}{\partial x^2} + k_f \epsilon \frac{\partial^2 T_f}{\partial x^2} \tag{41}$$

where A is the column cross-section area,

v_m is the specific volume of the solid,

ϵ is the porosity defined by $\epsilon \equiv A_f/A$,

C_p is the constant pressure specific heat,

and use has been made of the relations:

$$dh = C_p dT$$

$$\frac{d}{dt} = \frac{\partial}{\partial t} + V \frac{\partial}{\partial x} \tag{42}$$

$$V_f = \frac{\epsilon - 1}{\epsilon} V.$$

It is convenient to change variables because the thermodynamic properties of Gd are available [33,34] in the form of the entropy function

$$s = s(T,P,H)$$

at atmospheric pressure. From Ref. [35],

$$Tds = dh - \mu_o vHdM - vdP \tag{43}$$

so that for the metal in a constant pressure process,

$$T \frac{ds}{dt}\bigg|_p = \left[\frac{dh_m}{dt} - \mu_o v_m \frac{HdM}{dt} \right] \tag{44}$$

which is the factor to be transformed.

From calculus, at constant pressure,

$$T \frac{ds}{dt}\bigg|_p = T \left(\frac{\partial s}{\partial T} \right)_{p,vH} \frac{dT}{dt} + T \left(\frac{\partial s}{\partial vH} \right)_{p,T} \frac{d(vH)}{dt} \tag{45}$$

By this transformation of variables, the energy equation becomes, after letting $T_f = T_m$,

$$\left[\rho_m (1-\epsilon) T \left(\frac{\partial s}{\partial T} \right)_{p,\ vH} + \rho_f \epsilon C_{pf} \right] \frac{\partial T}{\partial t}$$

$$+ \left[\rho_m T \left(\frac{\partial s}{\partial T} \right)_{p,vH} - \rho_f C_{pf} \right] (1-\epsilon) V \frac{\partial T}{\partial x} \tag{46}$$

$$+ \left[\rho_m (1-\epsilon) T \left(\frac{\partial s}{\partial (vH)} \right)_{p,T} \left(\frac{\partial (vH)}{\partial t} + V \frac{\partial (vH)}{\partial x} \right) \right] = [k_f \epsilon + k_m (1-\epsilon)] \frac{\partial^2 T}{\partial x^2}$$

The factor

$$\frac{\partial (vH)}{\partial t} + V \frac{\partial (vH)}{\partial x}$$

is the total change in the field intensity observed at the magnetic material. The first term appears because the field appears to be time varying relative to the column due to the column motion. This term can be referenced to the magnet fixed coordinate (X) which removes the time varying component. Then

$$\left[\frac{\partial(vH)}{\partial t} + V \frac{\partial(vH)}{\partial x} \right] = \left[\frac{\partial(vH)}{\partial X} \right]_{V_{abs}} \tag{47}$$

where $V_{abs} = V_{col} + V$. V_{col} is the speed of the column relative to the magnet.

If $\epsilon = 1$, there is no Gd and the equation is

$$\rho_f C_{pf} \frac{\partial T}{\partial t} = k_f \frac{\partial^2 T}{\partial x^2} \tag{48}$$

as expected, then the energy change is due only to conduction in the fluid.

The boundary conditions are:

1. At the regenerator column ends:

   Initially adibatic, $\frac{\partial T}{\partial x} = 0$; then later isothermal, T = fixed.

2. At the Gd core ends:

   $T_{core} = T_{fluid}$

3. $$[k_m(1-\epsilon) + k_f\epsilon] \frac{\partial T}{\partial x}\Big|_{core} = k_f \frac{\partial T}{\partial x}\Big|_{fluid} \tag{49}$$

These conditions represent the continuity of temperature and heat flux.

Initially, the core and regenerator column are in thermal equilibrium at the temperature of the environment. The column ends are adiabatic so that the mechanical cycle of Fig. 1 will cause a temperature gradient to develop in the regenerator column, the left end being the hotter. The thermodynamic path is not a cycle because after each mechanical cycle, the temperature profile differs. However, eventually a thermodynamic cycle should result as the axial thermal conduction in the fluid limits the maximum temperature difference between the column ends.

After the column ends have reached temperatures suitable for refrigeration, the column ends are to be put into appropriate thermal contact with the source and sink of the refrigeration scheme. As a step in that direction, the first calculations included thermal reservoirs in contact with perfectly diathermal walls at the column ends. Heat transfer with the reservoirs occurs via conduction in the fluid and Gd.

Solution of the energy equation was implemented on a computer using a finite difference scheme. Non-dimensionalizing the equation was attempted. This proved to be very difficult due to non-constant coefficients and the lack of global geometric scales that can be used for references. Therefore a dimensional approach was used initially.

Some implementation difficulties, discussed more completely later [32], are

categorized as:

(1) Node Types.

The finite difference nodes are picked to be fixed relative to the regenerator column. As the core moves along the column the character of the nodes changes. Also, the core-fluid boundary is in general not at a node location. The numerical scheme must recognize different node types and use various schemes to calculate new temperatures. This leads to bookkeeping problems with the nodes.

(2) Stability and Convergence.

This is the usual problem with the ratio of step sizes. The space increment is chosen arbitrarily and the time increment Δt is computed to keep the coefficients in the numerical scheme positive. The increment Δt is also checked so that the core advances through the column by a set fraction of a space step.

(3) Convective Terms.

The convective terms $\left(\text{those with } \frac{\partial T}{\partial x}\right)$ had to be replaced with a one-sided upwind difference to improve stability. As V, the relative velocity between core and column changes sign, the $\frac{\partial T}{\partial x}$ terms change relative to the upwind directions. A higher order difference was also tried but did not improve stability.

Results

A. Adiabatic Column Ends, Initial Thermal Equilibrium

Some initial predictions from the model are given in Figs. 6-8. The component sizing was chosen independently of that in Section III. The regenerator column has a length of 1m, the core, 0.2m. The fluid is half water, half methyl alcohol by volume. The porosity of the core (open area/section area) is 0.80. The cylinder and ends of the regenerator are adiabatic. The vacuum field of the superconducting magnet is assumed constant in time and given by American Magnetics (see Appendix) for their 8 Tesla unit operating at 6T maximum.

At the start of the first cycle, the fluid and gadolinium are uniform in temperature at 295K. The end of the regenerator nearest to the magnet is 1m from magnet center and the core is near that end. After a half-cycle, the core and magnet are concentric, and the core is near the other end of the regenerator. The speed of the column relative to the magnet is 0.1m/s or zero. Also, the speed of the core relative to the magnet is 0.1m/s or zero. The cycle period is 37 seconds with no pauses and with velocities given by appropriate step functions.

Fig. 6 shows the temperature profile within the regenerator after 14.5 and 15 cycles. During this computer run, the minimum separation between the core and regenerator end was 5cm at each end. The column position, 0.00, marks the near end of the column at the start of a cycle. The drop in temperature at the

other end between the two profiles shows the cooling effect of removing the gadolinium from the magnet (followed by repositioning the column to complete the mechanical cycle). At present the model includes thermal conduction in the column, but excludes mixing. The gradients at the column ends reveal that axial conduction has a minor effect.

Fig. 7 shows the maximum and minimum temperatures in the column at each half-cycle. The nearly isothermal sections again reveal the minor effect of axial conduction. The curvatures suggest that asymptotes will be approached, but T_H-T_L is already close to the value found in the experiment by Brown and Pappel [3].

Fig. 8 gives the results of a run in which there is no dead space between the gadolinium and the ends of the regenerator. The temperatures at the column ends are now changing by a larger amount with each cycle.

B. Isothermal Column Ends, Initial Internal Thermal Gradients

The column is operated adiabatically as before until the highest temperature in the column goes above 310K and the lowest temperature in the column goes below 280K. Then reservoirs at 310K and 280K are coupled diathermally to the hot and cold ends, respectively. This is done computationally by holding the end nodes of the column at 310K and 280K. The core is assumed to travel the entire column length so at various times the core transfers thermal energy directly to the reservoirs. The heat transfer is

calculated from the temperature gradient and conductivity at each end for each increment of time. This is summed over a mechanical cycle to get the energy into the cold end and the energy rejected at the hot end. Once a thermodynamic cycle is achieved, the difference in these two quantities equals the work into the system.

Figure 9 shows the energy exchange with the reservoirs per mechanical cycle versus the number of successive mechanical cycles. The porosity is now 0.50. Q_H is the heat transfer at the sink per mechanical cycle, and Q_L is at the source. It appears that asymptotic values may occur, thus signalling the achievement of thermodynamic cycling.

In Fig. 10, the values of

$$\frac{Q_L}{Q_H - Q_L}$$

are plotted versus the number of successive mechanical cycles. The denominator does not represent the work involved because a thermodynamic cycle has not yet been obtained. However the data of Figs. 9 and 10 are not inconsistent with an asymptotic approach to a COP in the vicinity of the ideal COP of 9.33 for a Carnot refrigerator with reservoirs at 310K and 280K.

Such a limit will not be reached in this model because different sections of the Gd execute different thermodynamic paths. The thermodynamic paths are shown in Fig. 11 for three sections (left end, middle, right end) for the 30th mechanical cycle.

The program is stopped arbitrarily when both Q_H and Q_L in the Nth cycle differ by less than 1% from their respective values in the (N-1)th cycle. The same criteria for program cut-off was used in calculations starting with different core porosities. The results are given in Fig. 12, where

$$\frac{Q_L}{Q_H - Q_L}$$

is plotted versus core porosity. Any conclusions should be drawn cautiously since Figs. 9 and 10 suggest a closer approach to the asymptote may be needed. The result at low porosity may not be in error even though it exceeds the Carnot limit of 9.33, because a thermodynamic cycle has not been achieved. Clarification of this was not pursued because research has been started on a two-temperature model.

V. DISCUSSION/CONCLUSION

Large conventional chillers (1000 ton = 3.517 MW) have a capital cost near $150k, an electric operating use near 600 kW, an actual Coefficient of Performance of 5.86 and an ideal COP of 10 when operating between 280K and 308K.

The estimated system capital costs for ideal magnetic refrigeration systems of the same capacity become comparable as the cycle frequency approaches 10Hz, as shown in Table 2.

A significant counter trend is that the irreversibilities in the regenerator due to the relative motion of the fluid and the porous metal increase with cycle frequency. Such irreversibilites have not yet been treated in our modelling of the regenerator.

The capital costs for the magnetic refrigeration system appear to be driven by the cost and temperature-entropy characteristics of the magnetic material (Gd in this report) and by the structure/assembly costs of the magnet. Neither have been optimized. Magnetic materials of slightly less performance and considerably less cost are available and may be suitable. No attempt has been made to incorporate cost reductions which accompany high quantity manufacturing.

Future effort toward reducing the uncertainties in the magnet cost estimate may not be warranted until estimates of the COP of actual regenerators have been completed. The appropriate literature to do so seems scarce. In any case, an experimental program would be necessary.

VI. REFERENCES

1. Brown, G. V., "Magnetic Heat Pumping Near Room Temperature," Journal of Applied Physics, Vol. 47, 1976, pp. 3673-3680.

2. Brown, G. V., "Magnetic Stirling Cycles - A New Application for Magnetic Materials," IEEE Transactions on Magnetics, Vol. Mag 13, 1977, pp. 1146-1148.

3. Brown, G. V. and Papell, S. S., "Regeneration Tests of a Room Temperature Magnetic Refrigerator and Heat Pump," unpublished, 1978.

4. Weiss, Pierre, and Piccard, Auguste, "Sur un Nouveau Phenomene Magnetocalorique," Comptes Rendus Hebdomadaires Des Seances De L'Academie Des Sciences, Vol. 166, 1918, pp. 352-354.

5. Edison, T., British Patent 16709, 1887.

6. Tesla, W., U.S. Patent 428,057, 1890.

7. Debye, P., "Einige Bemerkungen zur Magnetisierung bei tiefer Temperature," Annalen Der Physik, Vol. 81, 1926, pp. 1154-1160.

8. Giauque, W. F., "A Thermodynamic Treatment of Certain Magnetic Effects. A Proposed Method of Producing Temperatures Considerably Below 1° Absolute," Journal of the American Chemical Society, Vol. 49, 1927, pp. 1864-1870.

9. Giauque, W. F. and MacDougall, D. P., Letter, Physical Review, Vol. 43, 1933, p. 768.

10. Heer, C. V., Barnes, C. B., and Daunt, J. G., "The Design and Operation of a Magnetic Refrigerator for Maintaining Temperatures Below 1 K," The Review of Scientific Instruments, Vol. 25, 1954, pp. 1088-1098.

11. Zimmerman, J. E., McNutt, J. D., and Bohm, H. V., "A Magnetic Refrigerator Employing Superconducting Solenoids," Cryogenics, Vol. 2, 1962, pp. 153-159.

12. Rosenblum, S. S., Sheinberg, H., and Steyert, W. A., "Continuous Refrigeration at 10 mK using Adiabatic Demagnetization," Cryogenics, Vol. 16, 1976, pp. 245-246.

13. Barclay, J. A. and Steyert, W. A., "Magnetic Refrigeration for Space Applications," Proceedings of International Cryogenic Engineering Conference, Genova, Italy, June 3-6, 1980, pp. 213-217.

14. Barclay, J. A. "Magnetic Refrigeration for Spacecraft Systems," 11th Intersociety Conference on Environmental Systems, ASME preprints, San Francisco, California, July 13-15, 1981.

15. Barclay, J. A., "An Analysis of Liquefaction of Helium Using Magnetic Refrigerators," Los Alamos National Laboratory, Report LA-8991, Dec. 1981.

16. Johnson, D. L., "Magnetic Refrigeration for Maser Amplifier Cooling," The Telecommunications and Data Acquisition Report 42-67, N82 20119, Jet Propulsion Laboratory, Pasadena, California, Nov.-Dec. 1981, pp. 29-38.

17. Mills, J. I., Kirol, L. D., and Van Haaften, D. H., "Magnetic Heat Pump Cycles for Industrial Waste Heat Recovery," 19th Intersociety Energy Conversion Engineering Conference, Vol. 3, San Francisco, California, August 19-24, 1984, pp. 1369-1374.

18. Van Geuns, J. R., "A Study of a New Magnetic Refrigerating Cycle," Phillips Research Reports Supplements, No. 6, 1966, pp. 1-105.

19. Brown, G. V., "Basic Principles and Possible Configurations of Magnetic Heat Pumps," ASHRAE Transactions, Vol. 87, Pt. 2, 1981, pp. 783-793.

20. Barclay, J. A., Moze, O., and Paterson, L., "A Reciprocating Magnetic Refrigerator for 2-4 K Operation: Initial Results," Journal of Applied Physics, Vol. 50, 1979, pp. 5870-5877.

21. Delpuech, C., Beranger, R., Bon Mardion, G., Claudet, G., and Lacaze, A. A., "Double Acting Reciprocating Magnetic Refrigerator: First Experiments," Cryogenics, Vol. 21, 1981, pp. 579-584.

22. Rosenblum, S. S., Steyert, W. A., and Pratt, W. P., Jr., "A Continuous Magnetic Refrigerator Operating Near Room Temperature," Los Alamos National Laboratory, Report LA-6581, May 1977.

23. Barclay, J. A. and Steyert, W. A., "Magnetic Refrigerator Development," Electric Power Research Institute, Final Report EL-1757, Project 7867-1, April 1981.

24. Pratt, W. P., Jr., Rosenblum, S. S., Steyert, W. A., and Barclay, J. A., "A Continuous Demagnetization Refrigerator Operating near 2 K and a Study of Magnetic Refrigerants," Cryogenics, Vol. 17, 1977, pp. 689-693.

25. Barclay, J. A., "Use of a Ferrofluid as the Heat-exchange Fluid in a Magnetic Refrigerator," Journal of Applied Physics, Vol. 53, 1982, pp. 2887-2984.

26. Nakogome, H. and Hashimoto, T., U.S. Patent 4,464,903, Aug. 14, 1984.

27. Larbalestier, D., Fisk, G., Montgomery, B., and Hawksworth, D., "High-field Superconductivity," Physics Today, Vol. 39, 1986, pp. 24-33.

28. Wilson, M., Superconducting Magnets, Oxford University Press, New York, 1983.

29. An approximation using Δs data ($q_L = T\Delta s$) from Brown's computer calculations for Fig. 5 of Ref. [34].

30. Conversations with various commercial suppliers.

31. Wilson, M., ibid., Fig. 12-17, "The best recorded critical-current densities for niobium-tin."

32. Smith, M. M. Ph.D., dissertation in progress, Georgia Tech.

33. Griffel, M., et al., "The Heat Capacity of Gadolinium from 15 to 355°K," Physical Review, Vol. 93, 1954, pp. 657-661.

34. Benford, S.M. and Brown, G. V., "T-S Diagram for Gadolinium Near the Curie Temperature," Journal of Applied Physics, Vol. 52, 1981, pp. 2110-2112.

35. Hatsopoulos, G. N., and Keenan, J. H., Principles of General Thermodynamics, Wiley, New York, 1965.

36. Booker, H. G. Energy in Electromagnetism, the Institute of Electrical Engineers, London and New York, Peter Peregrinus Ltd., New York, 1982.

37. Moon, F., Magneto-Solid Mechanics, Wiley, New York, 1984.

38. Chen, C. W., Magnetism and Metallurgy of Soft Magnetic Materials, North Holland, Amsterdam and New York, 1977.

39. Conversations with J. W. Brazell, Instructor in Mechanical Design, Georgia Institute of Technology.

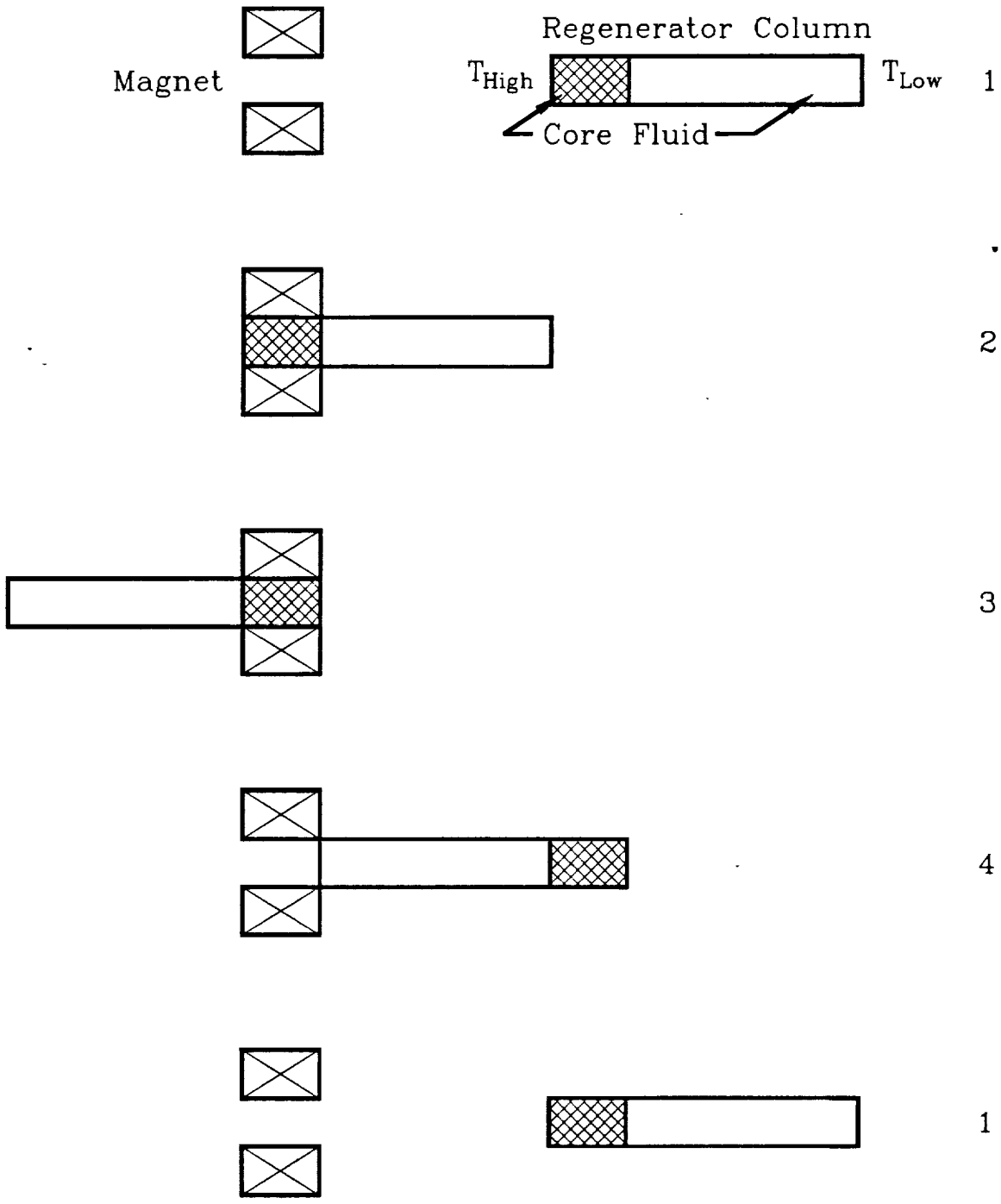

Fig. 1. Cycle Motion of a Reciprocating Magnetic Heat Pump.

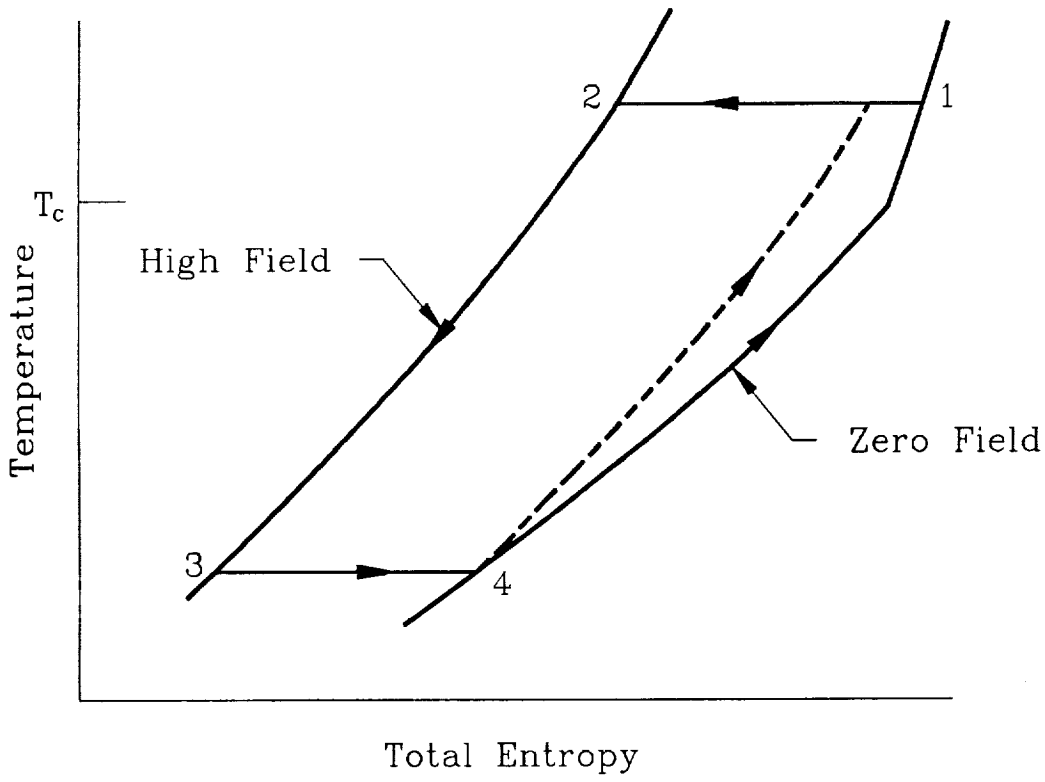

Fig. 2. A Theoretical Reversible Thermodynamic Cycle of the Magnetic Material in the Core

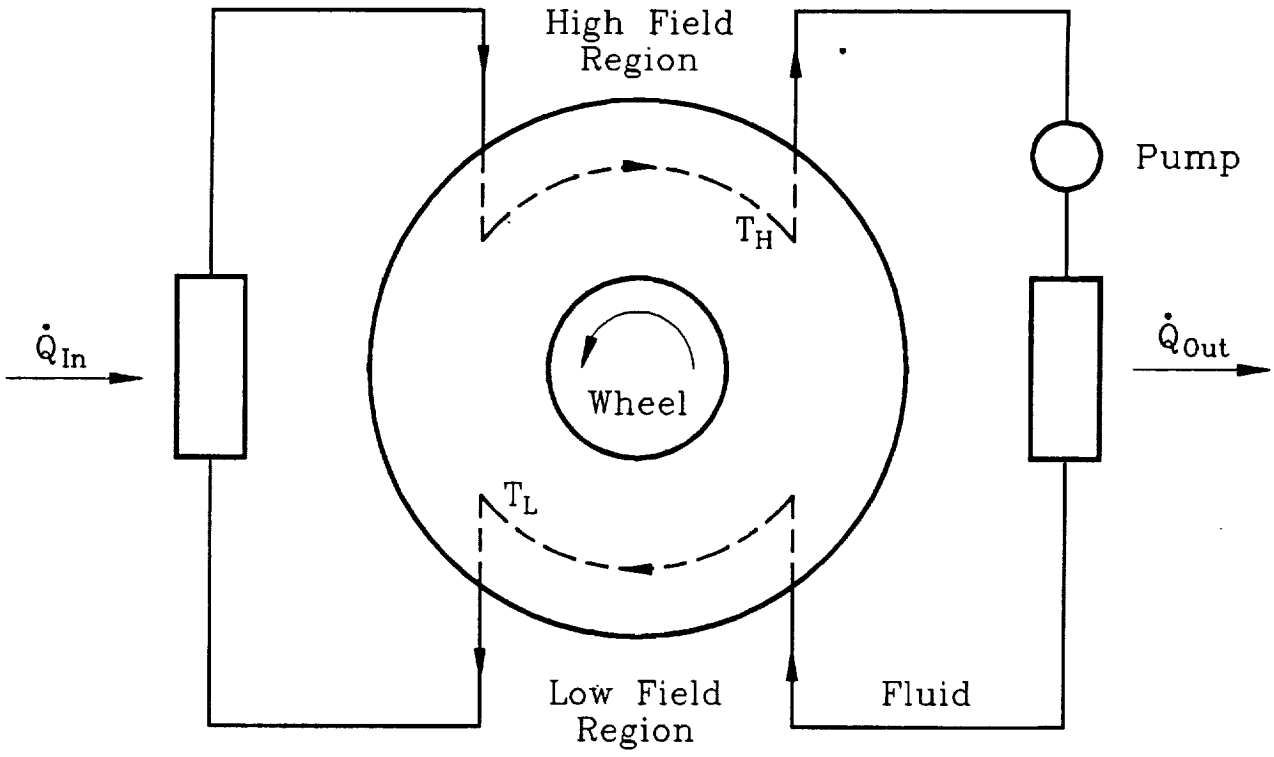

Fig. 3. Schematic of a Rotating Magnetic Heat Pump

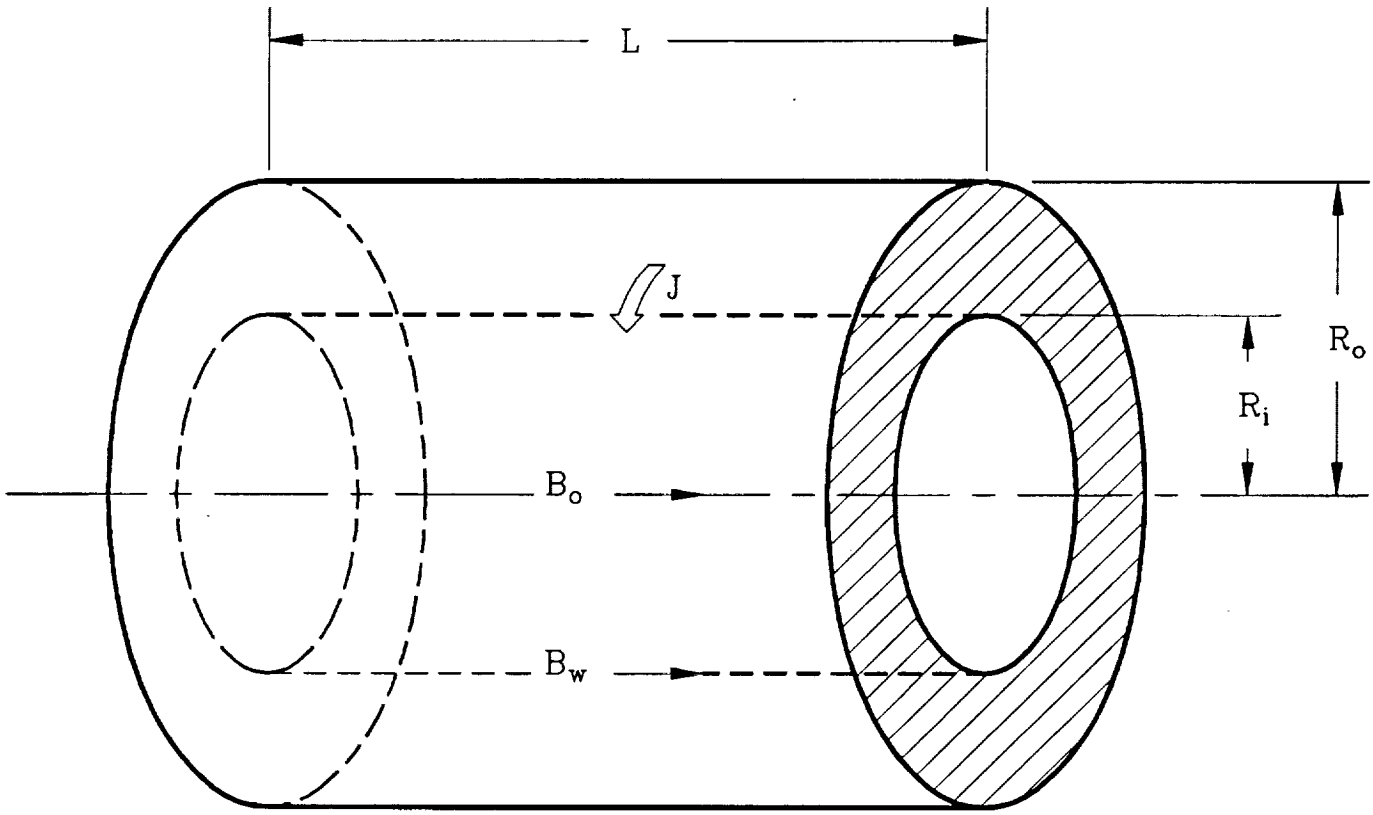

Fig. 4. Schematic of the Magnet Winding

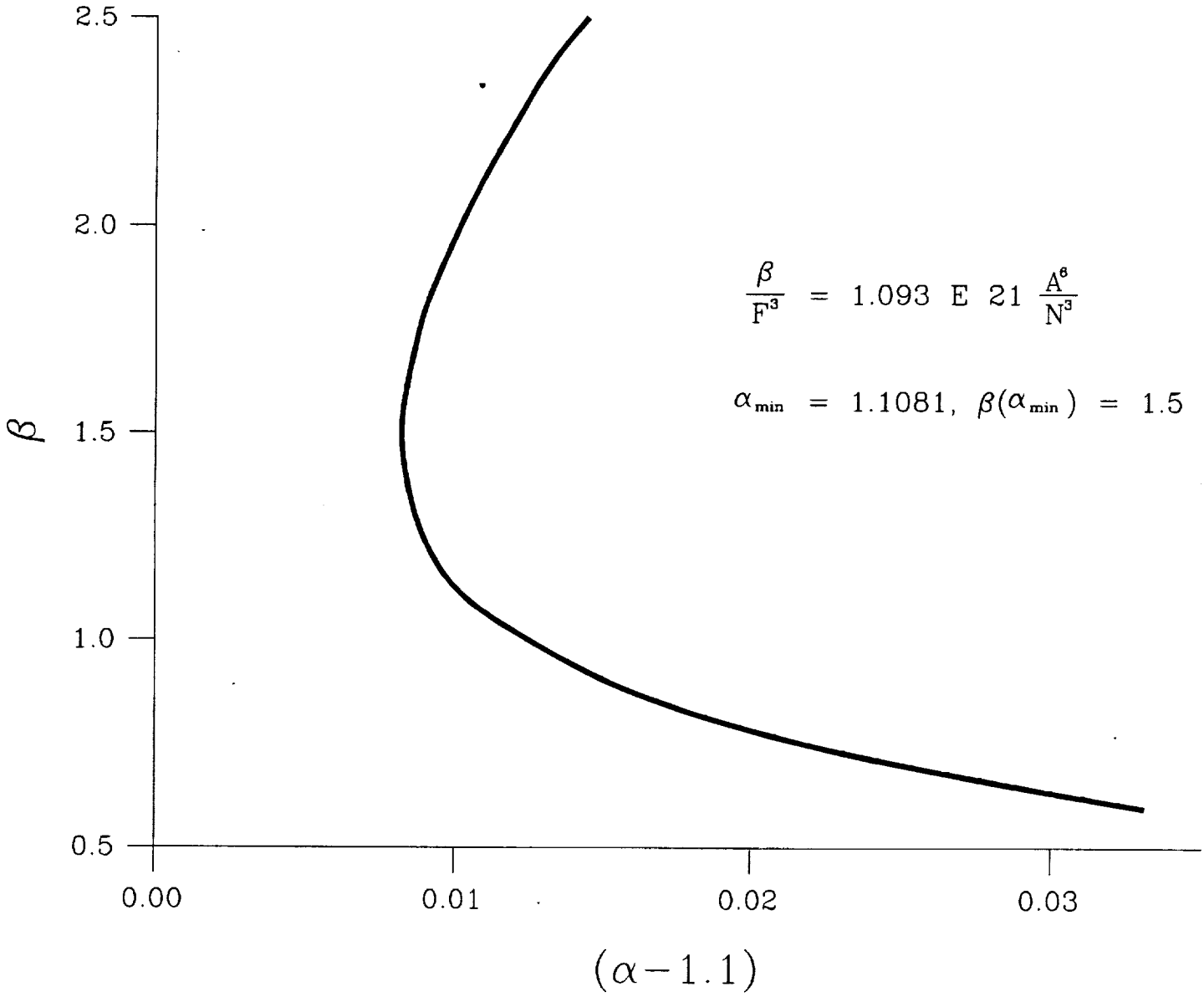

Fig. 5. The Shape Factors α, β Constrained By:

$$\frac{\beta}{F^3} = \text{Constant.}$$

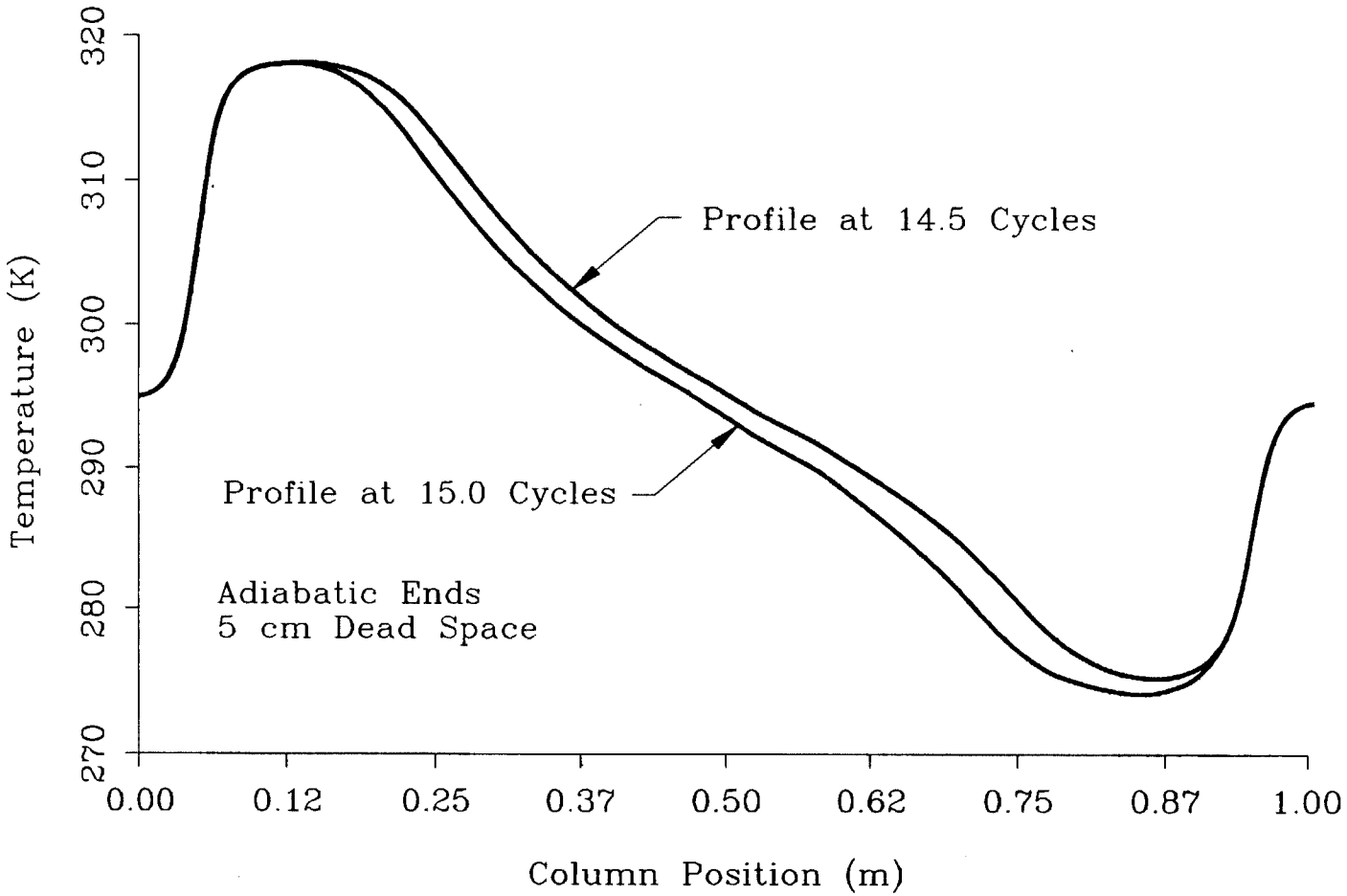

Fig. 6. Column Temperature Profile at 14.5 and 15 Cycles

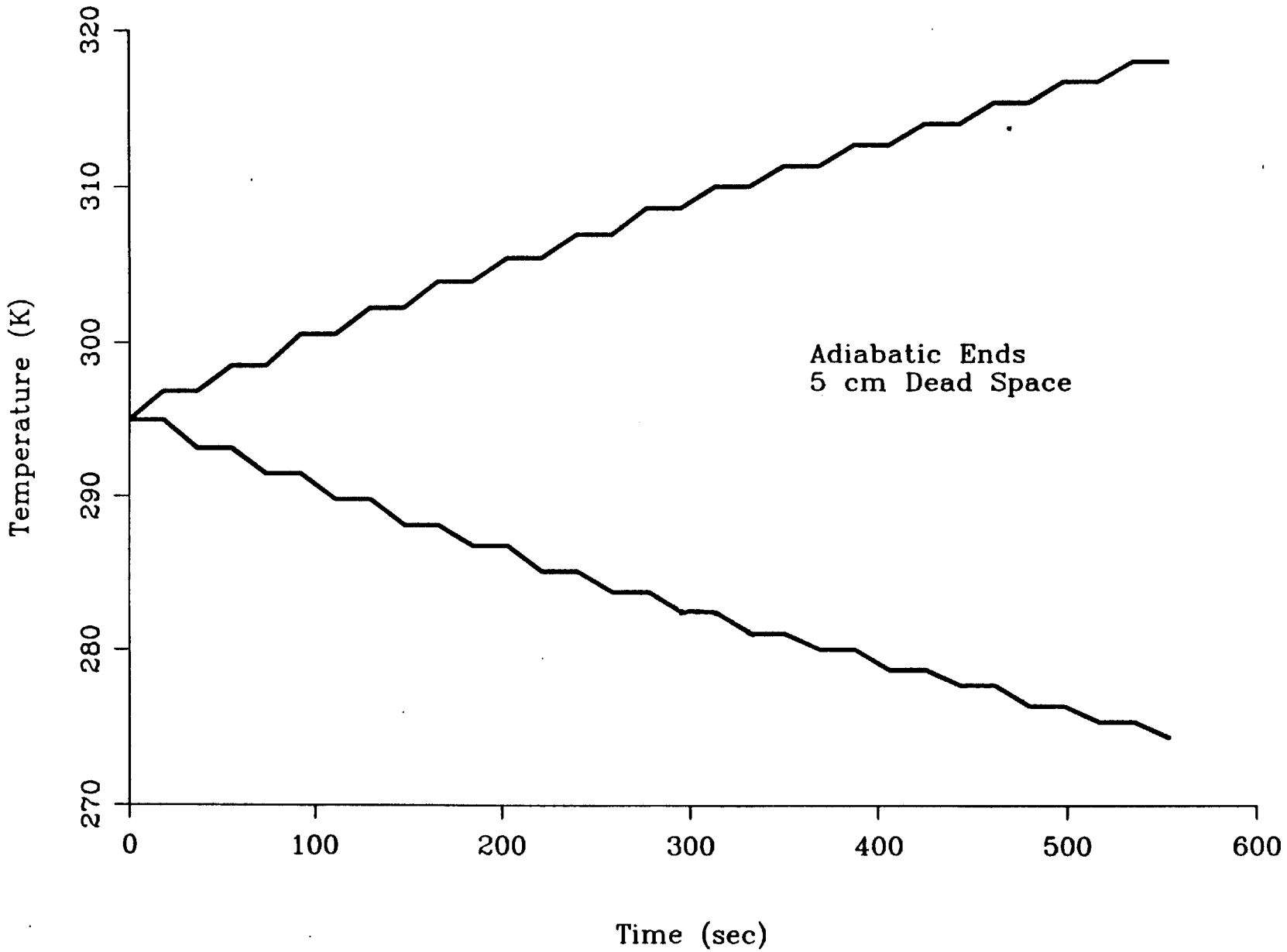

Fig. 7. Maximum and Minimum Temperatures in the Column versus Time.

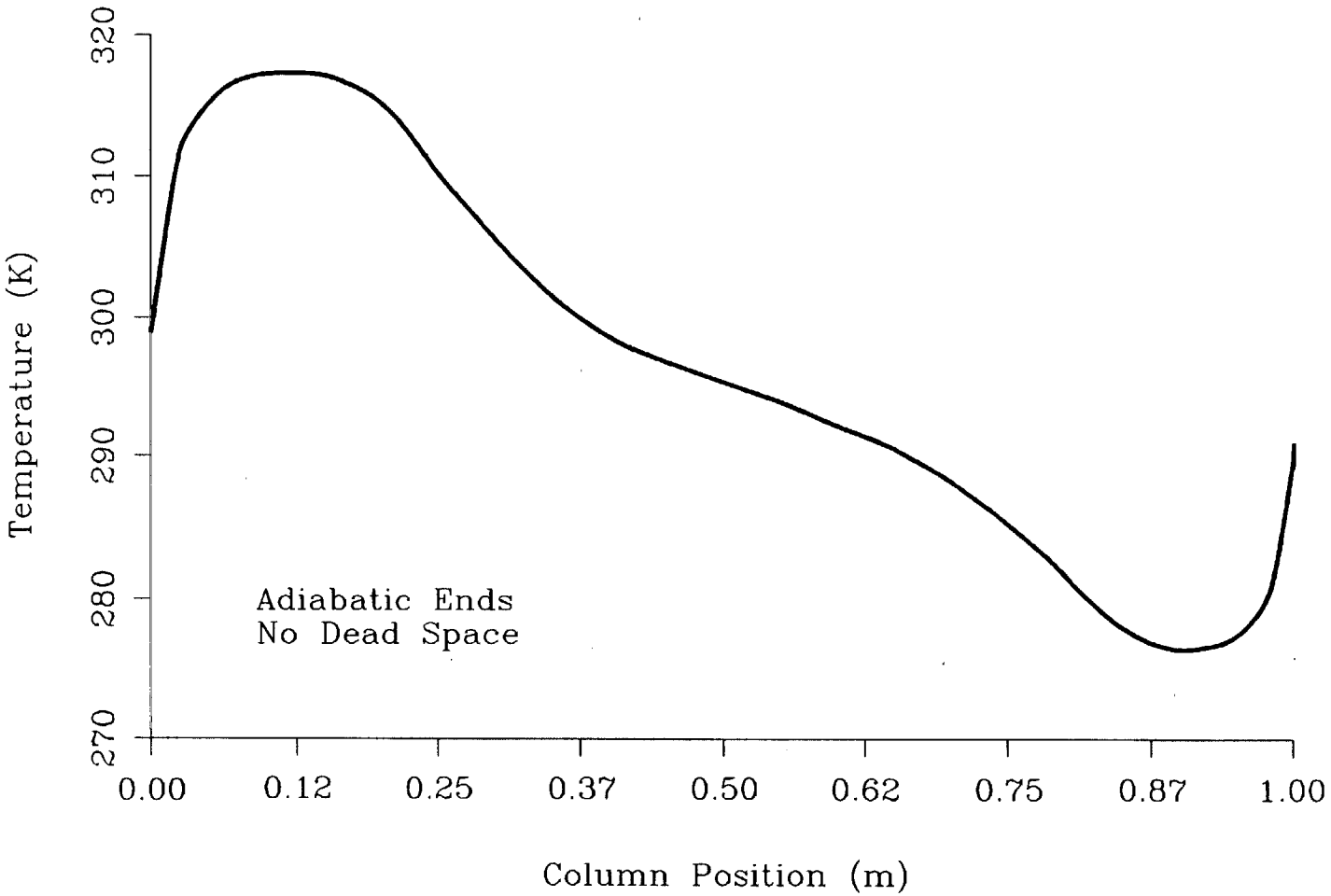

Fig. 8. Column Temperature Profile after 14.5 Cycles

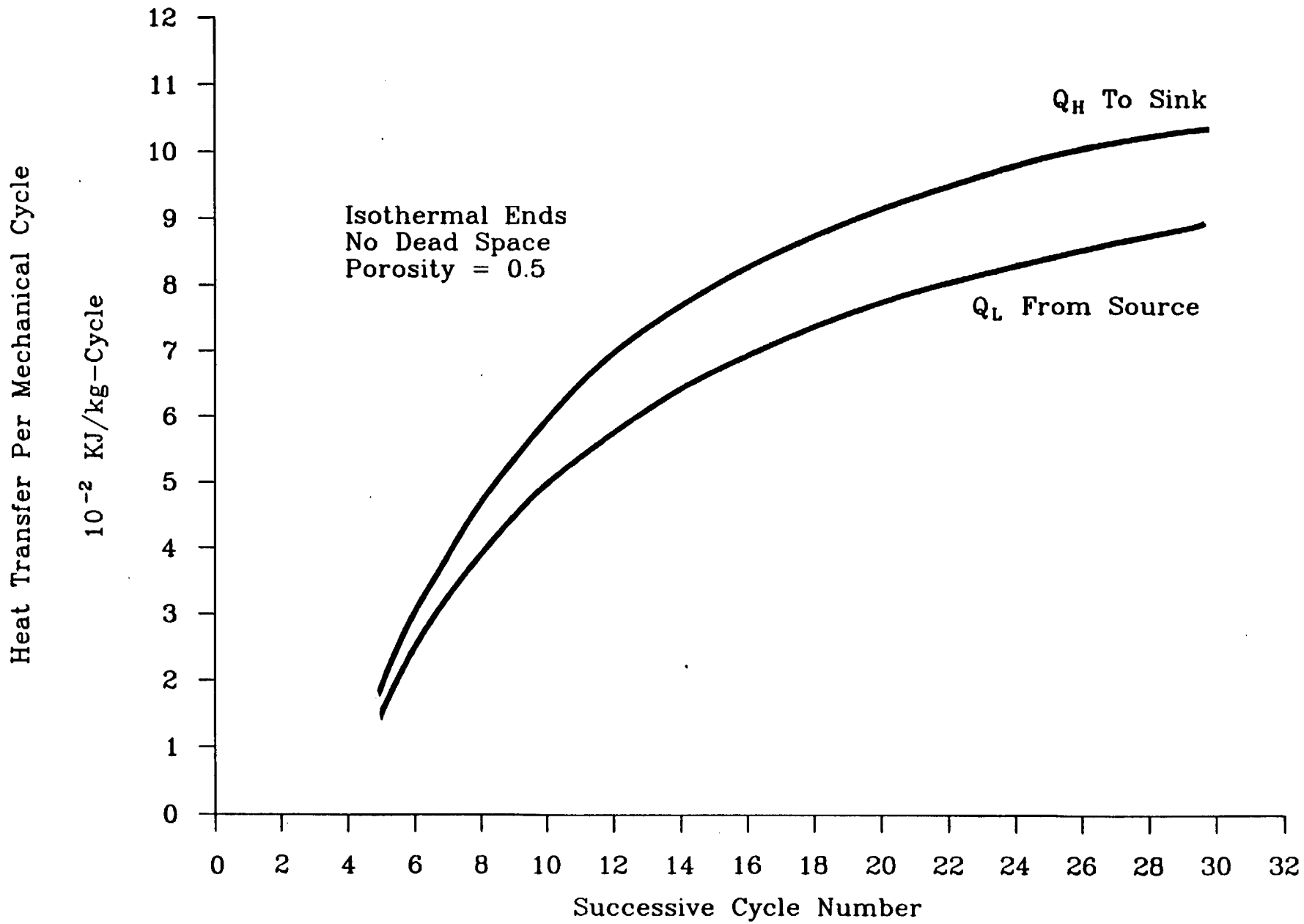

Fig. 9. Heat Transfer Per Cycle for Successive Mechanical Cycles

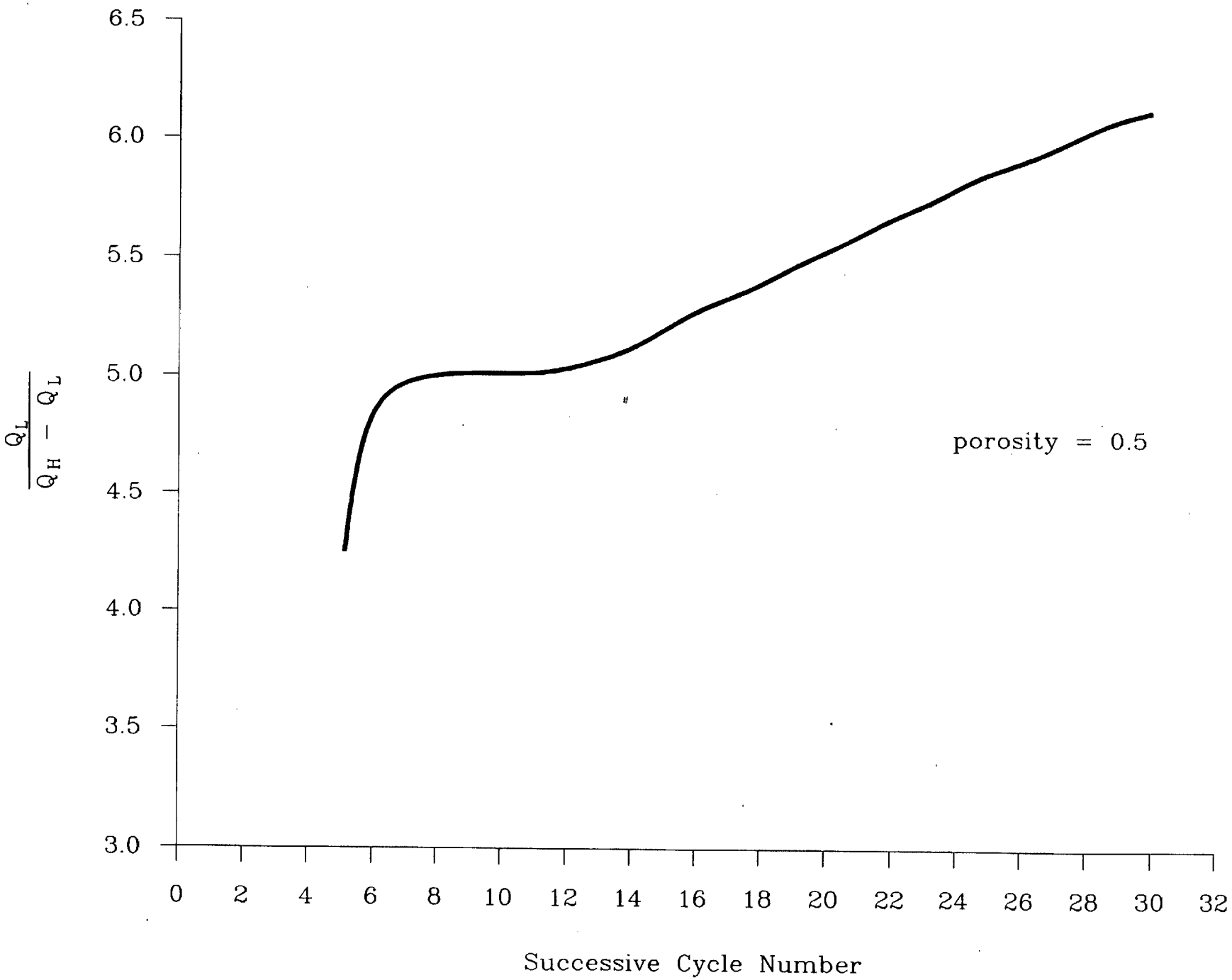

Fig. 10. $\frac{Q_L}{Q_H - Q_L}$ for Successive Mechanical Cycles

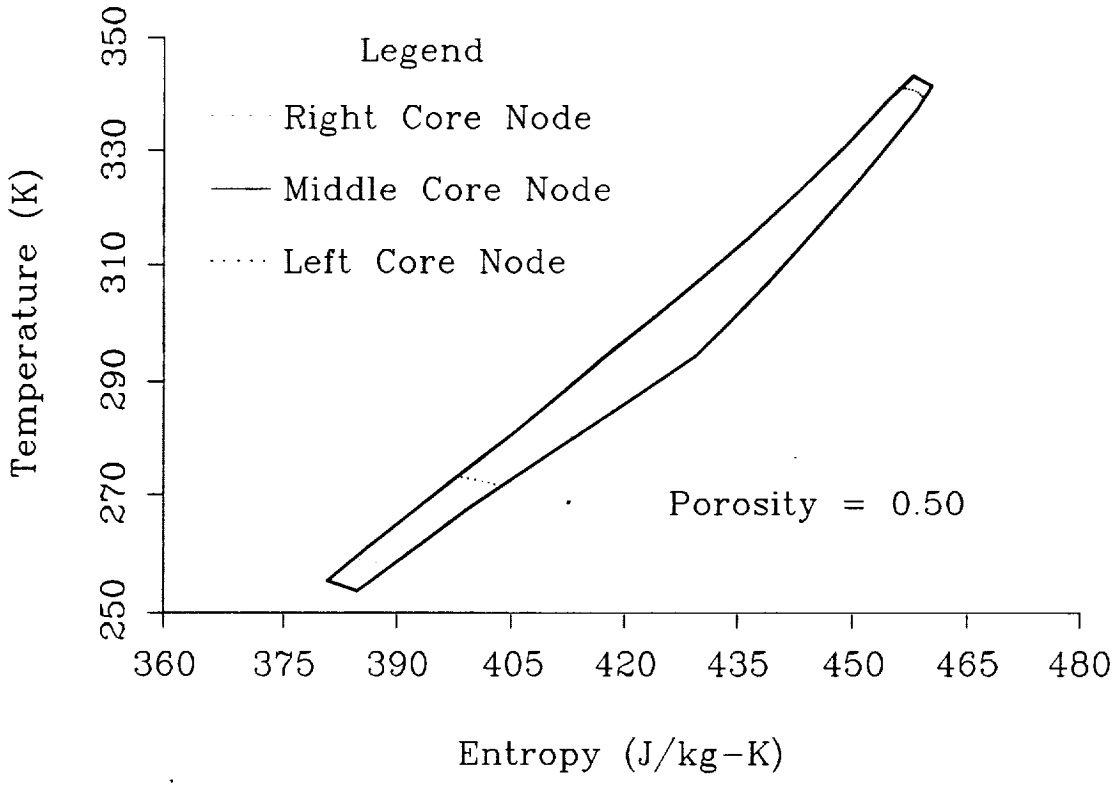

Fig. 11. T vs. S of Gd Core for Mechanical Cycle No. 30.

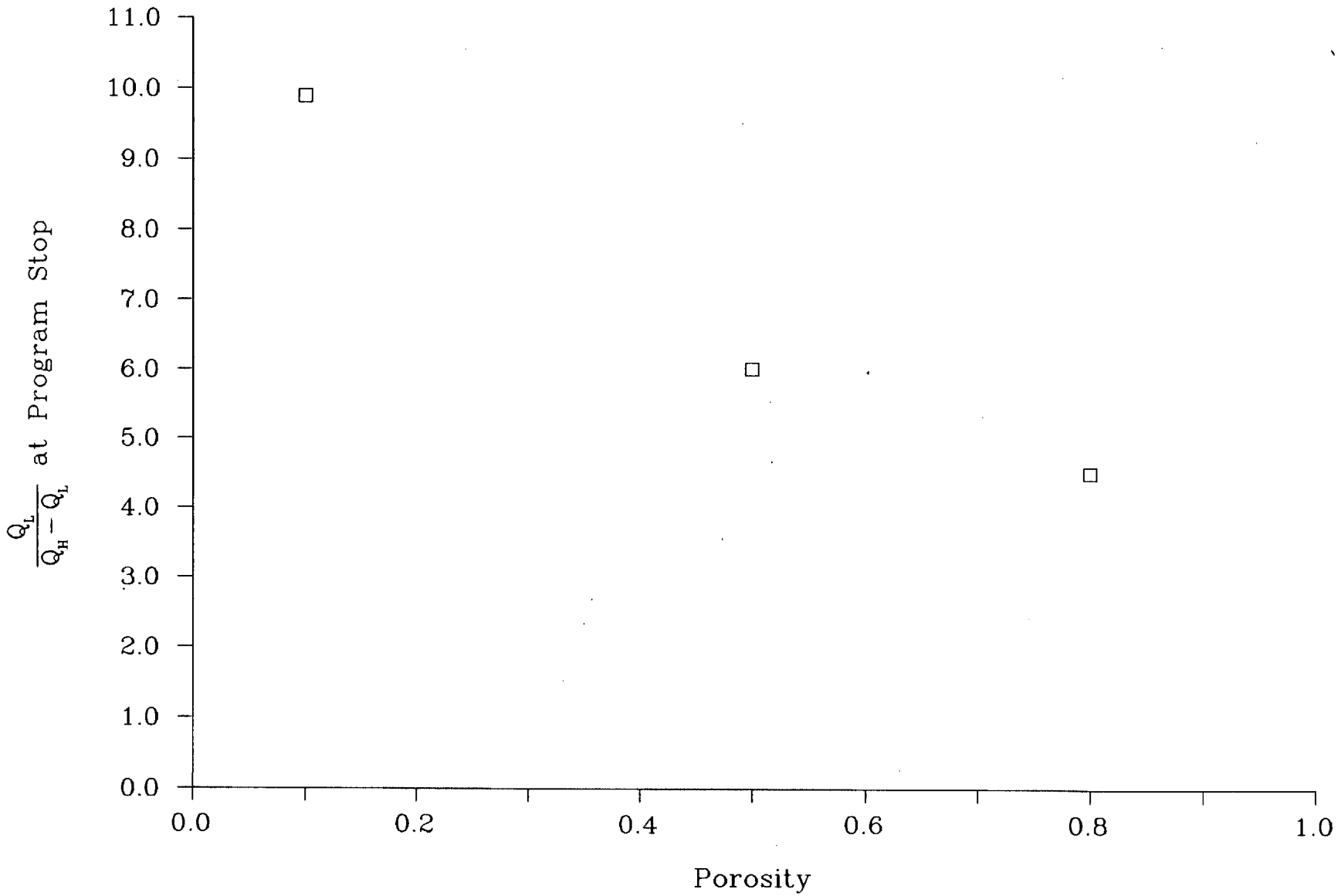

Fig. 12. $\frac{Q_L}{Q_H - Q_L}$ at Program Stop vs. Porosity of Gd Core.

APPENDIX

The magnetic field profile for the modelling of the regenerator is given below. The profile for an 8T magnet supplied by American Magnetics was arbitrarily multiplied by 3/4. The values are for the axis locations.

Distance from center,m	Field, Tesla
0.0000	6.000
0.0127	5.966
0.0254	5.850
0.0381	5.700
0.0508	5.275
0.0635	4.669
0.0762	3.776
0.0889	2.729
0.1016	1.829
0.1143	1.210
0.1270	0.818
0.1397	0.572
0.1524	0.413
0.1651	0.308
0.1778	0.236
0.1905	0.184
0.2032	0.147
0.2159	0.119
0.2286	0.098
0.2413	0.082
0.2540	0.0691
0.2667	0.059
0.2794	0.051
0.2921	0.045
0.3048	0.038